Electronic Supplementary Material (ESI) for ChemComm.

In-situ Electrochemical Mn Vacancies in CoMnHCF for High Level of Zinc Storage

Dan Wang [a] *& Ziyue Zhou,*[a] *Tengfei Ma,*[a] *Jinhua Zhang,*[a] *Yunhe Zhang,*[a] *Rui Ma,*[a] *Dapeng Zhang,**[a] *and Tingjiang Yan**[a]

[a] Key Laboratory of Catalytic Conversion and Clean Energy in Universities of Shandong Province, School of Chemistry and Chemical Engineering, Qufu Normal University, P. R. China

Experimental section

Chemical Synthesis.

First, 50 mL 0.5 mmol $CoCl_2$ and 50 mL 0.5 mmol $MnCl_2$ aqueous solutions were co-added in 1 mmol $K_4Fe(CN)_6$ aqueous solution drop by drop with strong stirring for 8 hours. The as-obtained precipitate was filtered, washed by deionized water and absolute ethanol, and dried in a vacuum oven at 60 ºC overnight. The obtained product was denoted as CoMnHCF. Meanwhile, CoHCF and MnHCF were prepared by the same method and compared with CoMnHCF just changing 0.5 mmol $CoCl_2$ + 0.5 mmol $MnCl_2$ to 1mmol $CoCl_2$ and 1 mmol $MnCl_2$, respectively. At the same time, we prepared $Co_{0.1}Mn_{0.9}HCF$, $Co_{0.3}Mn_{0.7}HCF$, $Co_{0.7}Mn_{0.3}HCF$, $Co_{0.9}Mn_{0.1}HCF$ by changing the mole ratio of $CoCl_2$ and $MnCl_2$ but maintain the whole quantity is 1 mmol.

Structure Characterization.

Powder X-ray diffraction (XRD) patterns were obtained from an X-ray diffractometer (Rigaku Mini Flex 600, Japan), using Cu Kα line (λ = 1.5418 Å) as the radiation source. TEM images and elemental mapping were obtained by a transmission electron microscope (JEOL JEM-2100, Japan). The SEM elemental mapping was obtained by a scanning electron microscope (Zeiss Sigma 500/VP, Germany). Fourier transform infrared (FTIR) spectra were recorded on an FTIR spectrophotometer (Thermo Fisher Nicolet iS20, USA). X-ray photoelectron spectroscopy (XPS) spectra were obtained from an X-ray photoelectron spectrometer (Thermo Fisher ESCALAB 250Xi, USA). The contents of Mn, Co and Fe were obtained by an inductively coupled plasma-atomic emission spectrometry (Aquion iCAU RQ, Germany).

Electrochemical Measurements

Electrochemical properties of CoMnHCF were evaluated in a glass electrolytic tank (50 mL), using zinc metal plate as the negative electrode, 1 M $ZnSO_4$ and 0.5 M Na_2SO_4 mixed aqueous solution (only 1 M $ZnSO_4$ for pure $ZnSO_4$ electrolyte) as the electrolyte (20 mL for every battery). When the electrolyte changed to pure Na_2SO_4 (0.5 M), the battery device is replaced to a three-electrode device (platinum plate as the counter electrode and saturated Ag/AgCl as the reference electrode). The positive electrode was made of 70 wt % prepared material, 20 wt % carbon powders, and 10 wt % polyvinylidene fluoride (PVDF). These materials were milled together in a trace of N-methyl-pyrrolidinone (NMP), then deposited onto a carbon paper pieces (NOS 1005, CeTech, Taiwan, 1 cm × 2 cm), and finally dried at 60 °C in vacuum. The mass loading of active material on every carbon paper piece is around 1~2 mg.

Galvanostatic charge-discharge profiles were measured by a battery test system (LANDT CT3002A, LANHE, China). Cyclic voltammograms (CV) were obtained on an electrochemical workstation (CHI660E, Chenhua Instruments Co., China). Electrochemical impedance spectra (EIS) were acquired from another electrochemical workstation (Autolab PGSTAT302N, Switzerland).

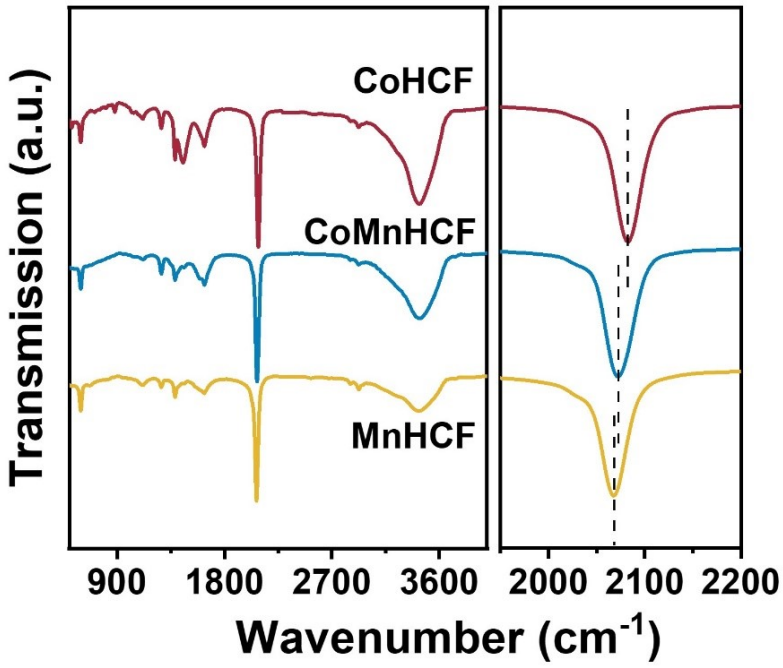

Figure S1. FTIR spectra of CoMnHCF, CoHCF and MnHCF.

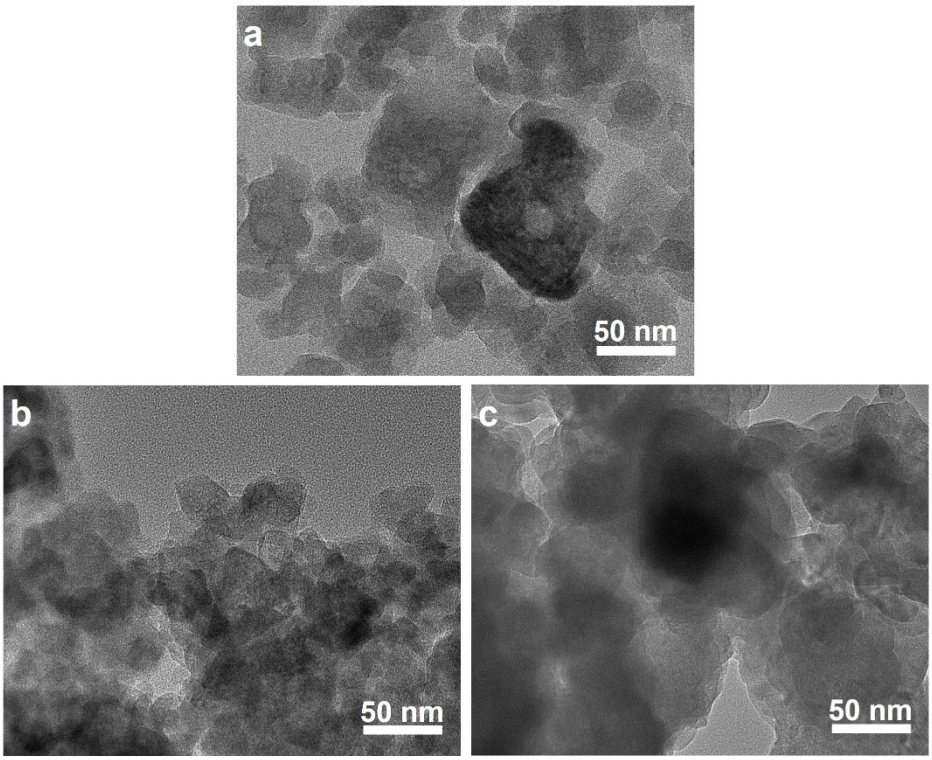

Figure S2. The TEM images of CoMnHCF, CoHCF and MnHCF.

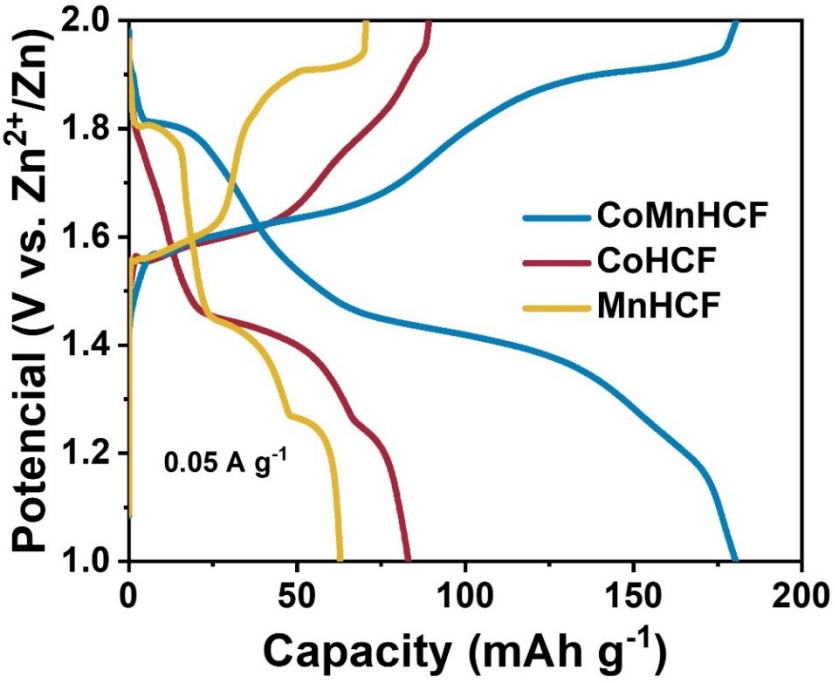

Figure S3. The charge-discharge profiles of CoMnHCF, CoHCF and MnHCF at 0.05 A g^{-1}.

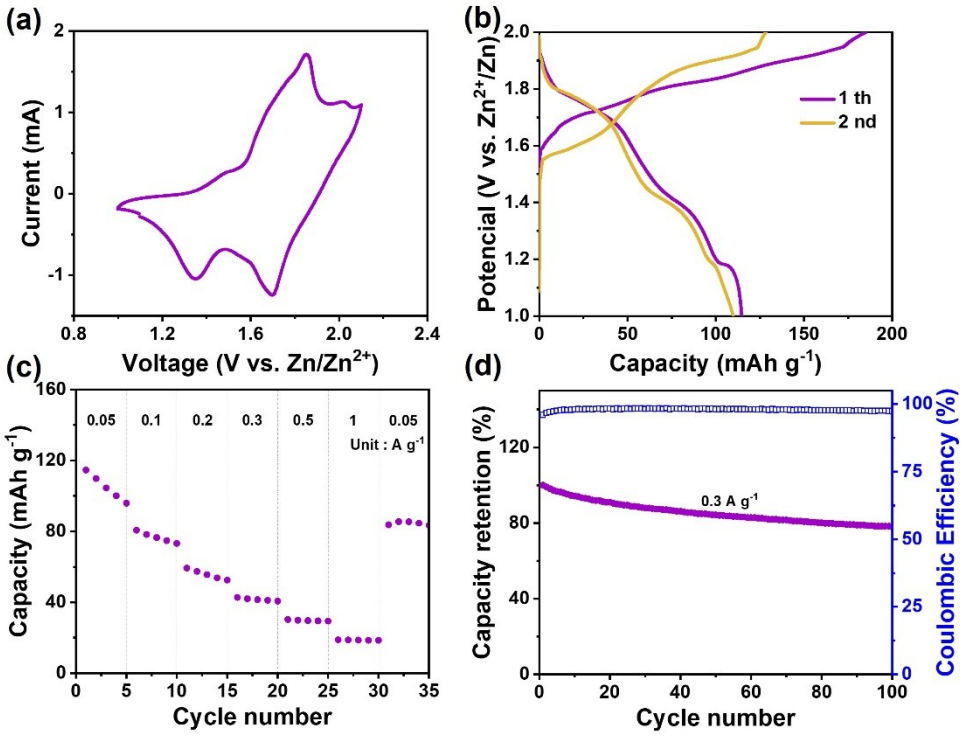

Figure S4. (a) The CV curves, (b) charge-discharge profiles, (c) rate performances and (d) cycle stabilities of CoMnHCF in coin cell.

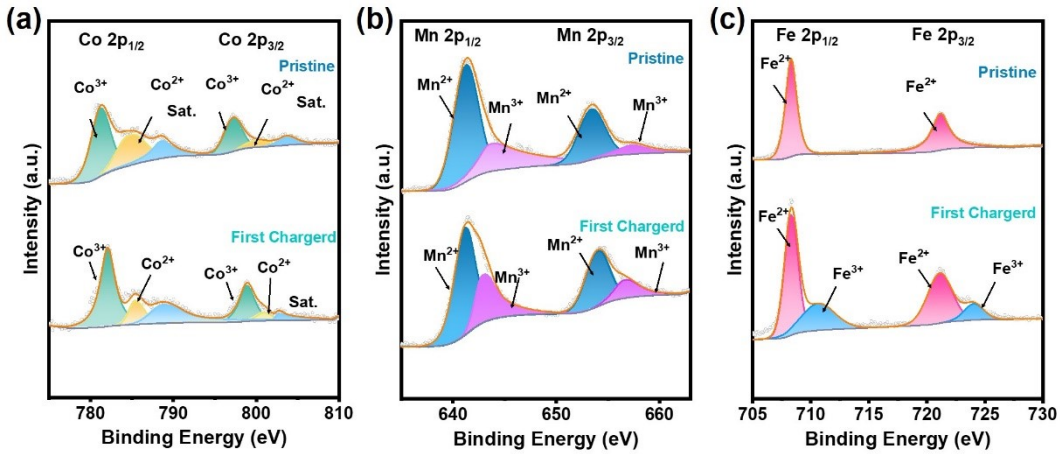

Figure S5. The XPS results of Co, Mn and Fe in CoMnHCF at pristine and after first charge process.

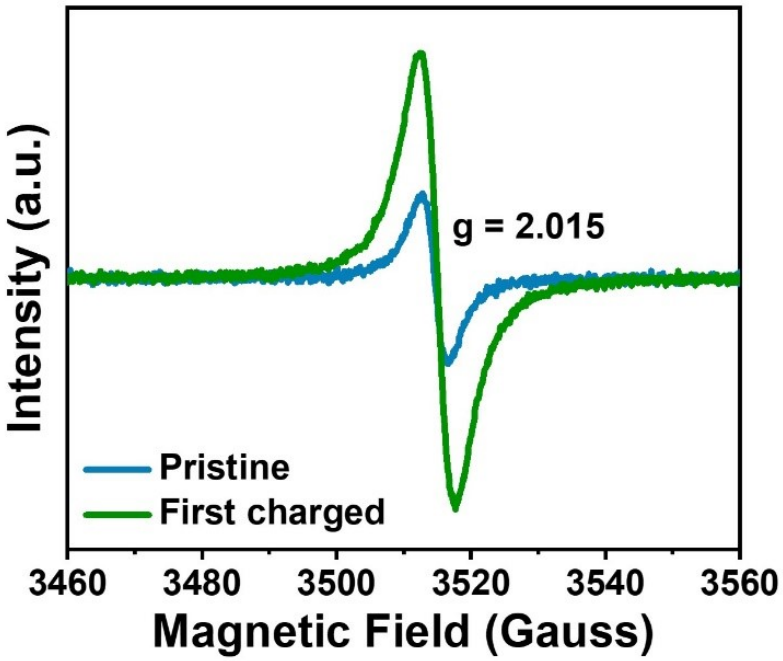

Figure S6. EPR results of CoMnHCF at pristine and after first charge process.

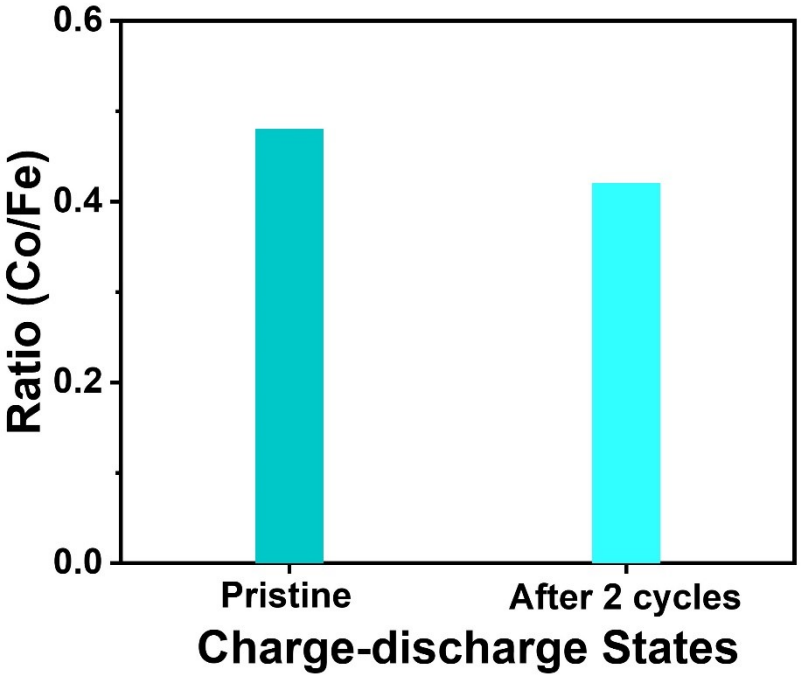

Figure S7. The atom ratios of Co/Fe in CoMnHCF at pristine state and after 2 cycles.

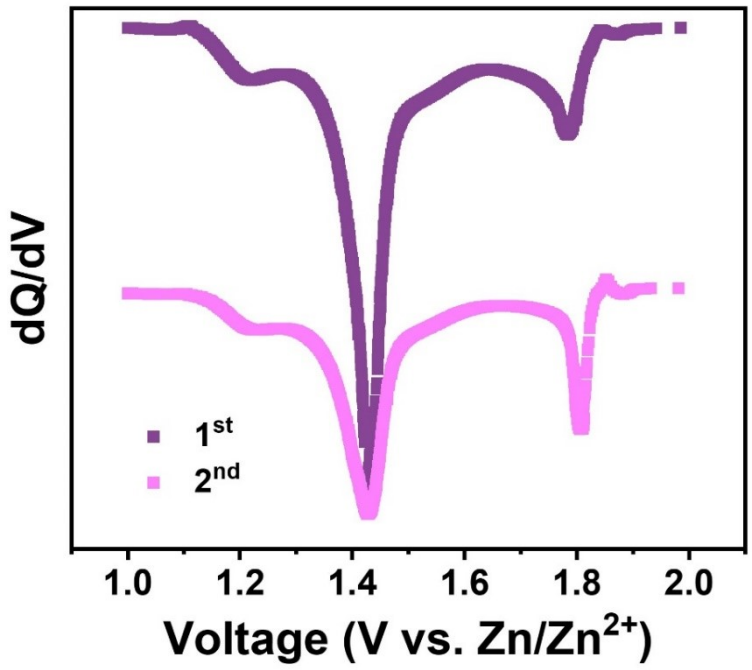

Figure S8. The dQ/dV results of CoMnHCF at first and second discharge process.

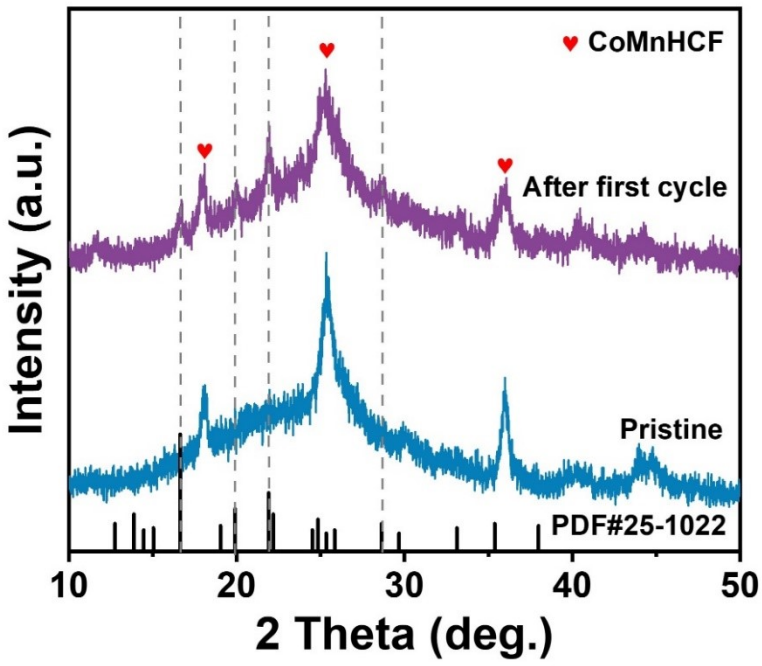

Figure S9. XRD patterns of CoMnHCF at pristine state and after first cycle.

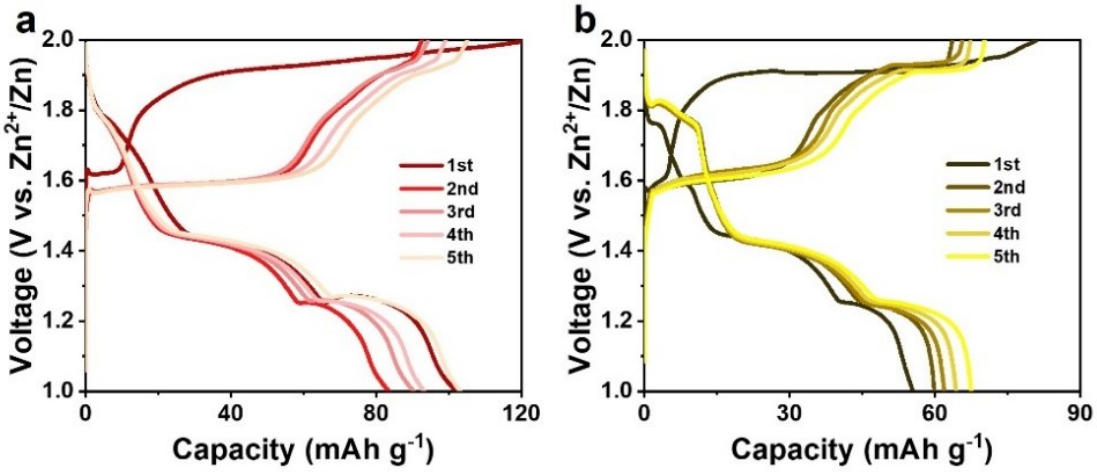

Figure S10. Charge-discharge profiles of CoHCF and MnHCF in $ZnSO_4/Na_2SO_4$ mixed electrolyte at first five cycles.

Both materials have a different electrochemical process and display a wide platform at ~1.9 V at first charging step, but the actual redox reactions are different. For CoHCF, K ions extract at this potential accompanied by the Fe^{2+} changing to Fe^{3+}, and the material structure does not change markedly due to the discharge profiles are almost remains the same from 1st to 5th cycle. However, the first discharge profile of MnHCF differs much with frequent four cycles in the discharge plateau at ~1.8 V. The reduction plateau in first cycle is located at 1.78 V derived from the Mn^{3+}/Mn^{2+} reaction, but this plateau changed to 1.8 V at second cycle and obviously extended, which is due to the participation of ZnHCF formed at first discharge process. Therefore, the oxide reaction at 1.9 V

for MnHCF contains not only the extraction of K^+ but also the dissolution of Mn^{3+}, which is much similar with that in CoMnHCF.

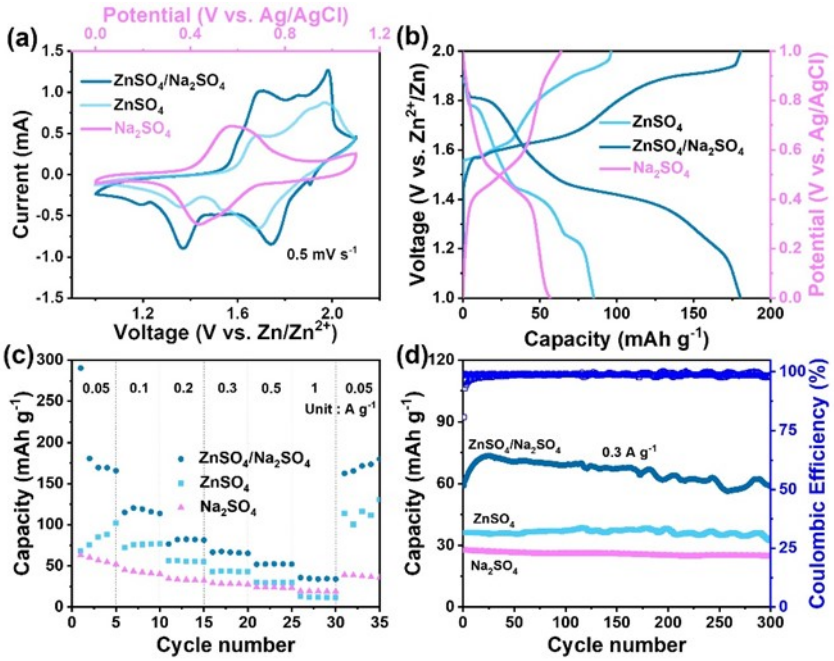

Figure S11. (a) The CV curves, (b) charge-discharge profiles, (c) rate performances and (d) cycle stabilities of CoMnHCF in $ZnSO_4/Na_2SO_4$, pure $ZnSO_4$ and pure Na_2SO_4 electrolyte.

CoMnHCF can deliver two redox couple in pure $ZnSO_4$ (Figure S11a), which is similar with that in mixed electrolyte, but along with a lower discharge capacity (85.1 mAh g^{-1}, Figure S11b). Meanwhile, in pure Na_2SO_4, the material has 56.7 mAh g^{-1} at discharge process with only one redox pair at 0.58/0.44 V (vs. Ag/AgCl). The discharge capacity of the material remains 75.9, 55.8, 43.4, 29.5 and 11.7 while the current density increases to 0.1, 0.2, 0.3, 0.5, and 1 A g^{-1}, respectively, and these results change to 42.3, 33.2, 28.3, 23.9 and 19.2 mAh g^{-1} in pure Na_2SO_4 (Figure S11c). All these results are poorer than those in mixed electrolyte. The cycle stabilities in pure $ZnSO_4$ and pure Na_2SO_4 are exhibited in Figure S11d. After 300 cycles at 0.3 A g^{-1}, the capacity retention in pure $ZnSO_4$ and pure Na_2SO_4 are 89.4 % and 90.1 %, worse than 99.3 % in $ZnSO_4/Na_2SO_4$ mixed electrolyte.

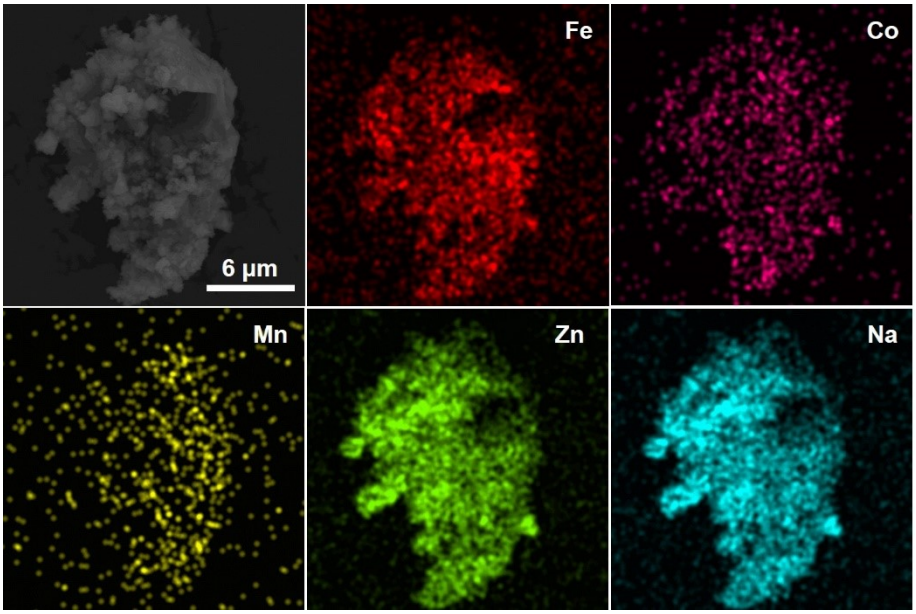

Figure S12. Elemental mapping of CoMnHCF after fully discharged.

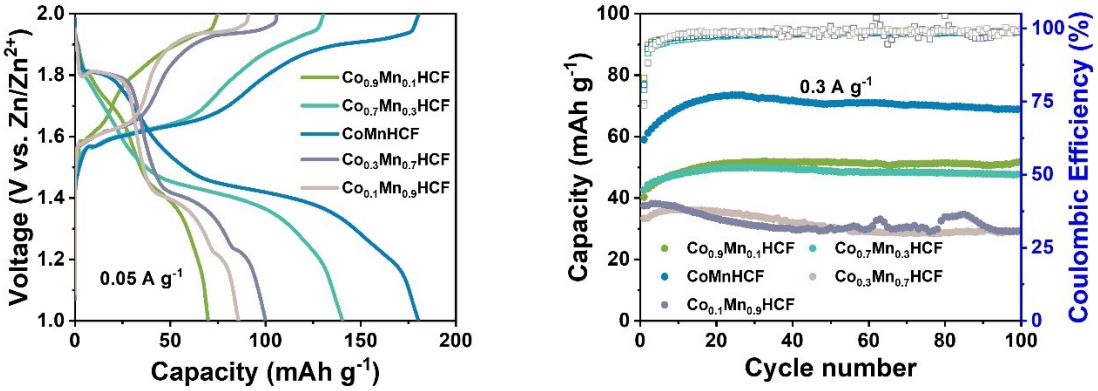

Figure S13. (a) The charge-discharge profiles and (b) cycle performances of CoMnHCF at different ratio of Co/Mn.

It is clear in Figure S8a that the discharge capacity of CoMnHCF is increasing when the ratio changes from 9/1 to 5/5 because of the density of in-situ Mn vacancies is growing. But the material structure would collapse rapidly when Co atoms are fewer than Mn atoms, leading to a smaller reversible capacity and bad cycle stability (Figure S8b).

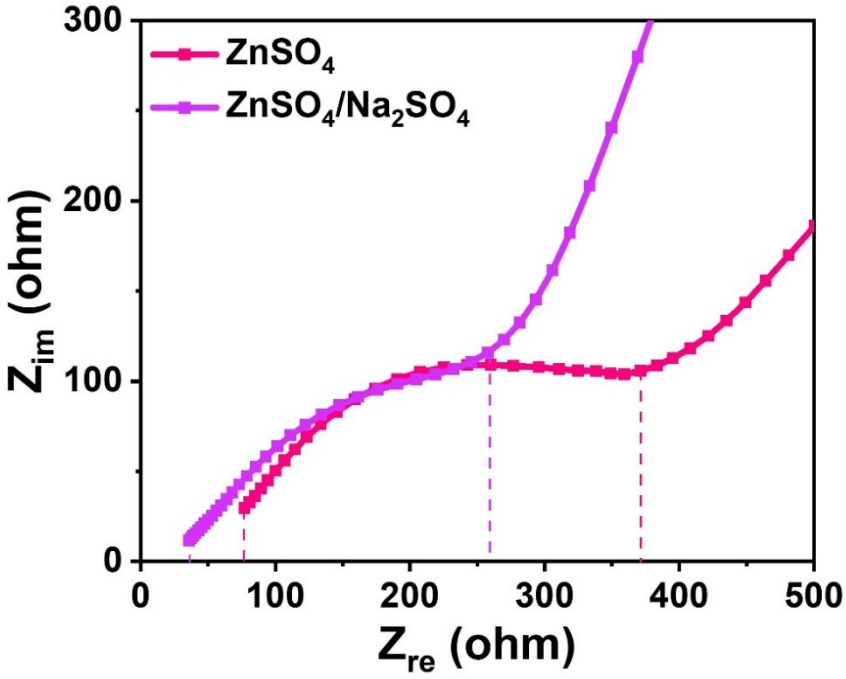

Figure S14. Nyquist plots of CoMnHCF at pure $ZnSO_4$ electrolyte and $ZnSO_4/Na_2SO_4$ mixed electrolyte.

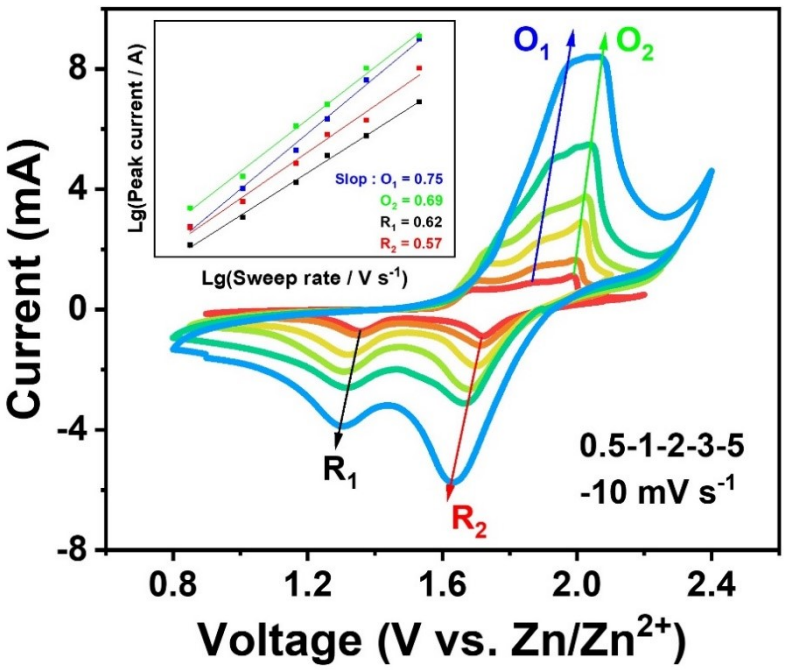

Figure S15. The CV curves of CoMnHCF at different sweep rate in $ZnSO_4/Na_2SO_4$ mixed electrolyte, the relationship between sweep rate and peak current is shown in the insert.

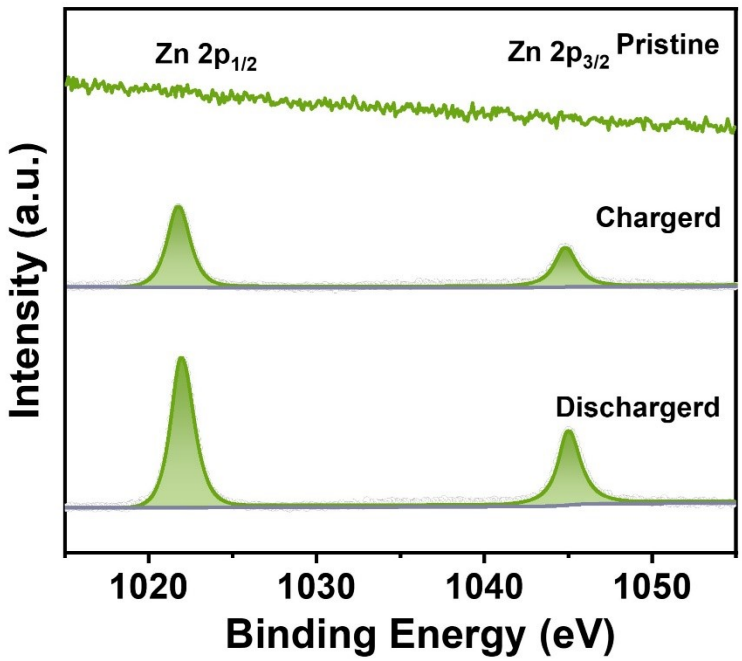

Figure S16. The high-resolution XPS results of Zn at pristine, fully charged and fully discharged states.

Table S1. The maximum discharge capacity of different PBAs in AZIBs.

PBAs	Electrolyte	Maximum capacity (mAh g^{-1})	References
CoHCF	$Zn(OTf)_2$	173.4	1
FeHCF	Na_2SO_4	78.5	2
VHCF	$Zn(CF_3SO_3)_2$	187	3
KZnHCF	KFSI + $Zn(CF_3SO_3)_2$	68.9	4
OH-rich MnHCF	$Zn(CF_3SO_3)_2$	132.8	5
NiHCF/RGO	$ZnSO_4$	94.5	6
CuCrHCF	$Zn(OTf)_2$@DTD	179.4	7
CoMnHCF	$ZnSO_4/Na_2SO_4$	180.4	This work

References

1. L. Ma, S. Chen, C. Long, X. Li, Y. Zhao, Z. Liu, Z. Huang, B. Dong, J. A. Zapien and C. Zhi, *Adv. Energy Mater.*, 2019, **9**, 1902446.
2. L. P. Wang, P. F. Wang, T. S. Wang, Y. X. Yin, Y. G. Guo and C. R. Wang, *J. Power Sources*, 2017, **355**, 18-22.
3. Y. Zhang, Y. Wang, L. Lu, C. Sun and D. Y. W. Yu, *J. Power Sources*, 2021, **484**, 229263.
4. W. Deng, Z. Li, Y. Chen, N. Shen, M. Zhang, X. Yuan, J. Hu, J. Zhu, C. Huang, C. Li and R. Li, *ACS Appl. Mater. & Interfaces*, 2022, **14**, 35864-35872.
5. Y. Tan, H. Yang, C. Miao, Y. Zhang, D. Chen, G. Li and W. Han, *Chem. Eng. J.*, 2023, **457**,

141323.
6. Y. Xue, Y. Chen, X. Shen, A. Zhong, Z. Ji, J. Cheng, L. Kong and A. Yuan, *J. Colloid Interface Sci.*, 2022, **609**, 297-306.
7. J. Zhao, H. Lu, J. Peng, X. Li, J. Zhang and B. Xu, *Energy Stor. Mater.*, 2023, **60**, 102846.